

Stable dinitrile end-capped closed-shell non-quinodimethane as donor, acceptor and additive of organic solar cells

Weixuan Liang,[†] Peng Liu,[†] Yiheng Zhang, Weiya Zhu, Xinyang, Tao, Zhicai He* & Yuan Li*

Institute of Polymer Optoelectronic Materials and Devices, State Key Laboratory of Luminescent Materials and Devices, South China University of Technology, Guangzhou, 510640, P.R. China

Non-fullerene acceptors exhibit great potential to improve photovoltaic performances of organic solar cells. The donors are open-shell and the highly efficient acceptors are closed-shell. However, it is important to further enhance chemical stability and device durability for future commercialization, especially for Y6-series small molecule acceptors with 2-(3-oxo-2,3-dihydroinden-1-ylidene)malononitrile (IC) type as ending group. In this work, an IC-free photovoltaic material YF-CN consisting of 2-fluoren-9-ylidenepropanedinitrile terminal was designed and synthesized by stille coupling. YF-CN exhibits enhanced photostability and improves morphological compatibility with the binary PCE10:Y6 blend. The moderate energy level makes YF-CN could serve as a multifunctional material, such as donor, acceptor and the third component. When adding YF-CN as second donor into PCE10:Y6 system, an improved power conversion efficiency of 12.03% was achieved for as-cast device. Importantly, the ternary PCE10:YF-CN:Y6-devices showed enhanced storage durability maintaining 91% of initial PCE after the 360 hours. This work provides new perspective to understand the open-shell and closed-shell structure of donors and acceptors, as well as promising design concept of stable IC-free acceptors for organic solar cells.

organic solar cell, non-fullerene acceptor, photostability, ternary, bulk heterojunction

1 Introduction

Organic solar cells (OSCs) are considered to be the next potentially commercialized photovoltaic technology owing to their advantages including light weight, flexibility and large-scale fabrication via solution processing [1-5]. The active layer of conventional OSCs usually comprises a binary blend bulk heterojunction (BHJ) of electron donor and acceptor, which plays a critical role in determining the performances of the devices [6-7]. In recent 10 years, as immense efforts have been dedicated to the molecular design of non-fullerene acceptors (NFAs), the power conversion efficiencies (PCEs) of single-junction OSCs have made great progress [8-17].

Different from the binary OSCs, the ternary OSCs appear to an available strategy to extend light absorption, facilitate exciton dissociation and optimize the morphology, leading to the improvement of photovoltaic performances [18-26]. Cascade energy alignment could be achieved by introducing third component with suitable energy levels, which is beneficial to suppress charge recombination [27-28]. Another significant function of third component is to improve the compatibility and miscibility with the binary blend film [29-

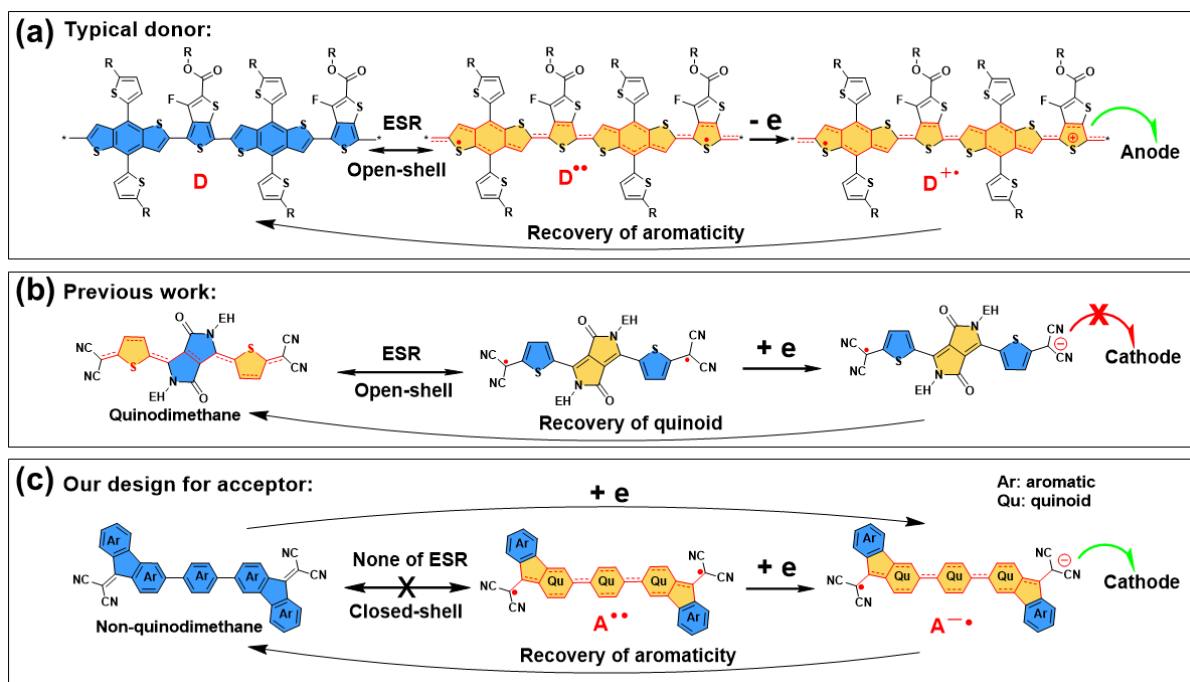
31]. However, it should be noted that the addition of third component also might make more complex morphology and create difficulties on morphology control for some ternary systems [32]. Selecting the appropriate third component, PCEs of surpassing 18% have been reported for efficient ternary OSCs, which indicates tremendous potential for development [33-39].

In addition to high efficiency, the device stability is also an important factor for solar cells to be commercialized [40-42]. For Y6-series non-fullerene solar cells, the key to achieve high device stability is to stabilize the microstructure of blend film [43]. Furthermore, most of emerging NFAs containing - (3-oxo-2,3-dihydroinden-1-ylidene)malononitrile (IC)-type terminals are synthesized by Knoevenagel condensation reaction, which would make them prone to decompose under persistent light irradiation [44-49]. The development of IC-free NFA is still very challenging, to date.

In our previous work, we have disclosed the open-shell radical character of donor-acceptor (D-A) type organic semiconductors [50-53]. As presented in **Scheme 1**, the donor of OSCs including PCE10 and small molecules show quinoidal radical resonance structure which will produce radical cation and recover aromatic neutral form during the

[†]These authors contributed equally to this work.

*Corresponding authors (email: celiy@scut.edu.cn, zhicaihe@scut.edu.cn)



Scheme 1 (a) The resonance structure of typical open-shell donor PCE10 and the formation of radical cation during the operation of OSCs. (b) Previous resonance structure of open-shell CN-TDPP based on 2,5-bis(2-ethylhexyl)-3,6-di(thiophen-2-yl)-2,5-dihydropyrrolo-[3,4-c]pyrrole-1,4-dione (TDPP) and the formation of radical anion during the operation of OSCs. (c) Our design on closed-shell acceptor and the formation of radical anion during the operation of OSCs.

operation of OSCs (**Scheme 1a**) [54-57]. In previous work, the p-quinodimethane CN-TDPP is typical diradicaloid with an open-shell singlet ground state and it showed poor performance in OSCs as the radical anion will be stabilized while it formed aromatic resonance structure (**Scheme 1b**) [51-52]. Based on these considerations above, we proposed a new strategy to construct the closed-shell aromatic (non-quinodimethane) backbone with dinitrile end-capping groups for the design of NFAs in OSCs (**Scheme 1c**) and this will produce expected high stability than IC-based NFAs. It is noteworthy that the radical anion will more readily recover into the aromatic neutral form comparing the p-quinodimethane in **Scheme 1b** due to the well-known aromatic stabilization energy effect detected in previous Chichibabin type diradicaloids [51].

Herein, we reported an IC-free organic small molecule named YF-CN with facile synthesis steps by changing the terminal group of Y6 into 2-fluoren-9-ylidenepropanedinitrile. Compared with Y6, YF-CN shows good photostability and higher energy levels. The achievement of PCEs for binary OSCs based on PCE10:YF-CN and YF-CN:Y6 blend suggests that YF-CN exhibits unprecedented and unique bipolar charge accepting capability, that is, it can either work as an electron acceptor or as an electron donor, in non-fullerene organic solar cells. This also makes it effective as the third component to improve the ternary OSCs device efficiency of the classic material system of PCE10:Y6, resulting in an elevated PCE of 12.03% without solvent additive and posttreatment. The

improved PCE of the ternary OSCs origins from the increased V_{OC} and J_{SC} compared with PCE10:Y6-based OSCs. This is supposed to rise as a consequence of the enhanced exciton separation, optimized morphology and improved the charge transport mobility facilitated by the addition of third component. Furthermore, better storage stability was realized in the ternary devices whose PCE exhibited a slight decrease of merely 9% after storing 360 h because of the enhanced microstructure stability of ternary active layer.

2 Results and discussion

The synthesis of YF-CN consists of two steps, which is described in the Support Information. Nuclear magnetic resonance (NMR) spectra and the high-resolution matrix-assisted laser desorption/ionization time of flight (MALDI-TOF) mass spectrum of the intermediate and YF-CN are shown in **Figure S1-S5**. **Figure 1a** presents the chemical structures of active materials PCE10, YF-CN and Y6. The optical and electrochemical parameters of PCE10, YF-CN and Y6 are summarized in **Table 1**. Compared with the solution, YF-CN film exhibited an absorption peak at 687 nm that is red-shifted by ~70 nm (**Figure S6**), indicating the existence of strong π - π interactions in the solid film [58]. The YF-CN film has broad absorption in the range of 500~800 nm with the absorption onset located at 838 nm, leading to the optical bandgap of 1.48 eV. To assess the photostability

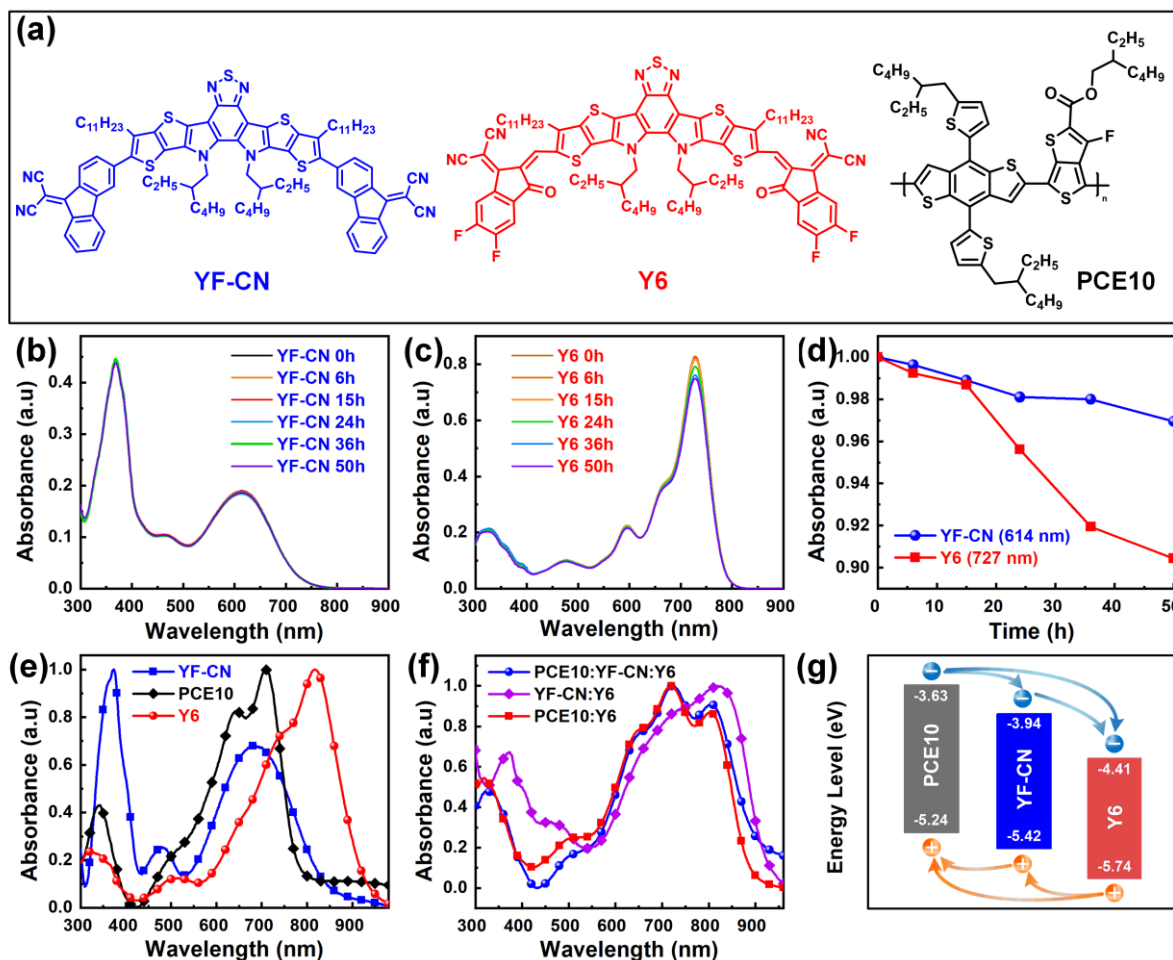


Figure 1 (a) Molecular structure of the acceptor YF-CN, PCE10 and Y6. Solution aging time-dependent UV-vis absorption of (b) YF-CN and (c) Y6 upon 100W tungsten lamp. (d) The change of absorption intensity of YF-CN and Y6 under different aging time. (e) UV-vis absorption spectra of films of above materials. (f) UV-vis absorption spectra of blend films. (g) Energy levels of PCE10, YF-CN and Y6 and the paths of charge transfer.

Table 1 The optical and electrochemical parameters of PCE10, YF-CN and Y6.

Materials	$\lambda_{\text{peak}}^{\text{film}}$ (nm)	$\lambda_{\text{onset}}^{\text{film}}$ (nm)	E_g^{opt} (eV)	HOMO (eV)	LUMO (eV)
PCE10	707	772	1.61	-5.24	-3.63
YF-CN	370, 687	838	1.48	-5.42	-3.94
Y6	816	932	1.33	-5.74	-4.41

of YF-CN and Y6, we conducted their absorption decay test in chlorobenzene solutions under illumination of 100W tungsten lamp. As displayed in **Figure 1b-1d**, YF-CN exhibited high photostability with almost constant absorption intensity, while a significant attenuation was found in the absorption of Y6. The improved photostability can be attributed to the advantages of robust C-C single bonds, rather than the delicate exocyclic C=C bonds [49]. As for the absorption of films, when compared with Y6, the absorption peak of YF-CN exhibits an apparent blue-shift (**Figure 1e**) because of the weaker electron withdrawing ability of ending group, which leads to attenuated intramolecular charge transfer interaction [59]. In addition, the absorption of YF-CN exhibits partial overlap with the absorption of PCE10. Therefore, compared with the absorption position of

PCE10:Y6, the introduction of the third component YF-CN partially replacing PCE10 does not change the light absorption obviously in the ternary PCE10:YF-CN:Y6 blend films (**Figure 1f**). The donors are open-shell, and the efficient NFAs are closed-shell including YF-CN, ITIC, and Y6 that exhibited none or extremely weak ESR signal, while the poor acceptor CN-TDPP shown in scheme 1b possessed a strong ESR signal [51-52].

The highest occupied molecular orbital (HOMO) energy levels of materials were measured by cyclic voltammetry (CV) method (**Figure S7**). The lowest unoccupied molecular orbital (LUMO) energy levels were calculated on the basis of the optical band gap and the corresponding HOMO energy levels. **Figure 1g** shows the corresponding energy levels of the three photovoltaic materials and the paths of charge transfer

Table 2 The Photovoltaic performance of the binary and ternary devices (the Average Values for eight Devices), under the Illumination of AM 1.5 G, 100 mW cm⁻².

Active Layer	V _{oc} (V)	J _{sc} (mA cm ⁻²)	FF (%)	PCE (%)
PCE10:YF-CN	0.839	4.97	33.78	1.41 (1.32±0.09)
YF-CN:Y6	0.785	5.53	33.17	1.44 (1.39±0.05)
PCE10:Y6	0.673	25.32	64.19	10.93 (10.81±0.12)
PCE10:YF-CN:Y6	0.683	27.92	63.11	12.03 (11.68±0.34)

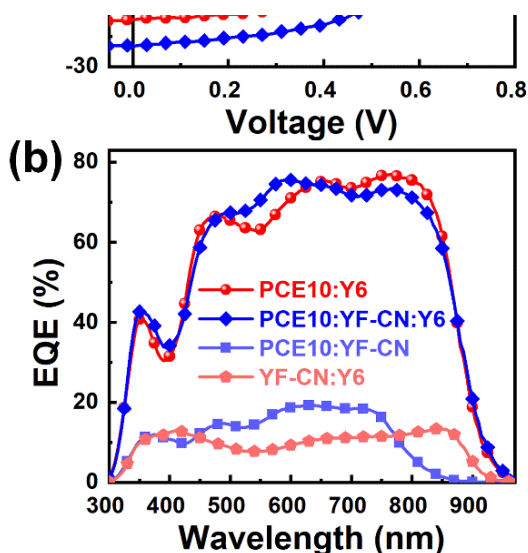


Figure 2 (a) J–V curves and (b) EQE spectra for YF-CN-based binary and ternary devices.

transfer. The LUMO and HOMO levels of YF-CN were determined to be -3.94 eV and -5.42 eV, respectively, the equation $E_{\text{LUMO}} = E_{\text{HOMO}} + E_g$. The cascaded energy alignment could be formed in the ternary OSCs, which is beneficial to the facilitation of charge transfer and exciton dissociation [60-61]. The work function of YF-CN was also determined to be 5.67 eV by ultraviolet photoelectron spectroscopy (**Figure S8**).

To evaluate the exciton dissociation and charge transfer in the blend, the photoluminescence (PL) spectra of PCE10, YF-CN, Y6 and their blend films were measured. As shown in **Figure S9**, PCE10 neat film and Y6 neat film exhibited a PL emission peak at 750 nm and 845 nm, respectively. When incorporating YF-CN into the blend, the PL intensity of binary films like PCE10:YF-CN and YF-CN:Y6 were significantly quenched, suggesting the efficient exciton dissociation at both PCE10:YF-CN and YF-CN:Y6 interface [62]. Moreover, compared with PCE10:Y6 film, the ternary PCE10:YF-CN:Y6 blend film displayed a greater extent of quenching approaching 100% owing to the role of YF-CN as a cascade material. These results indicate the progressive function of YF-CN for boosting charge transfer ability in the ternary blend and the possible application for ternary OSCs with YF-CN as third component.

To examine the photovoltaic performance of YF-CN, the OSCs were fabricated with a conventional device structure of ITO/PEDOT:PSS/active layer/PDINO/Ag. The relevant current density–voltage (J–V) curves are shown in **Figure 2a** and the photovoltaic performances are summarized in Table 2. Firstly, we using PCE10 as donor and YF-CN or Y6 as acceptor to investigate photovoltaic properties of binary OSCs. The PCE10:Y6 (1:1.5)-based as-cast devices exhibited a PCE of 10.93%, along with a high open-circuit voltage (V_{oc}) of 0.673 V and a short-circuit current density (J_{sc}) of 25.32 mA cm⁻² and a fill factor (FF) of 64.19%. The PCE10:YF-CN (1:1.5)-based device annealed at 110°C gave a rather low PCE of 1.41% but a higher V_{oc} of 0.839 V, with weaker J_{sc} and FF (4.97 mA cm⁻² and 33.78%, respectively). The larger V_{oc} of PCE10:YF-CN-based device could be ascribed to the higher LUMO level of YF-CN than that of Y6, while the lower J_{sc} may be due to the weaker absorption of YF-CN. On the other hand, considering the high HOMO energy level of YF-CN, we also fabricated all-small-molecule OSCs based on YF-CN:Y6 (1:1) binary active layer with thermal annealing, which provided a surprising PCE of 1.44%. The above results demonstrate the efficient charge transfer at PCE10:YF-CN and YF-CN:Y6 interface, and indicate the developmental potential of YF-CN both as donor and acceptor of OSCs.

Furthermore, we adjusted the photovoltaic performance of the ternary OSCs based on PCE10:Y6 with YF-CN as third component and a constant weigh ratio of Y6, varying the proportion between PCE10 and YF-CN in the blend. Detailed photovoltaic results for the ternary OSCs with different YF-CN contents are shown in **Figure S10** and summarized in Table S1. As a result, the ternary as-cast OSCs with PCE10:YF-CN:Y6 of ratio 0.8:0.2:1.5 yield a highest PCE of 12.03%, with synergistic enhancement in V_{oc} and J_{sc} (0.683 V and 27.92 mA cm⁻², respectively) but a slightly lower FF of 63.11%, compared with the above PCE10:Y6-based devices. The enhanced values of photovoltaic performances can be attributed to the terraced energy level alignment and optimized morphology in the ternary active layers [36].

The external quantum efficiency (EQE) of the OSCs were measured to investigate the spectral responses of the devices (**Figure 2b**). The devices based on PCE10:Y6 showed a broad photoelectrical response in the wavelength range of 300-1000 nm. When incorporating YF-CN as third component, the EQE values of ternary OSCs were slightly enhanced in the band between from 500 to 600 nm, which is in accordance with the enhancement of current density. For PCE10:YF-CN, YF-CN:Y6, PCE10:Y6 and as-cast

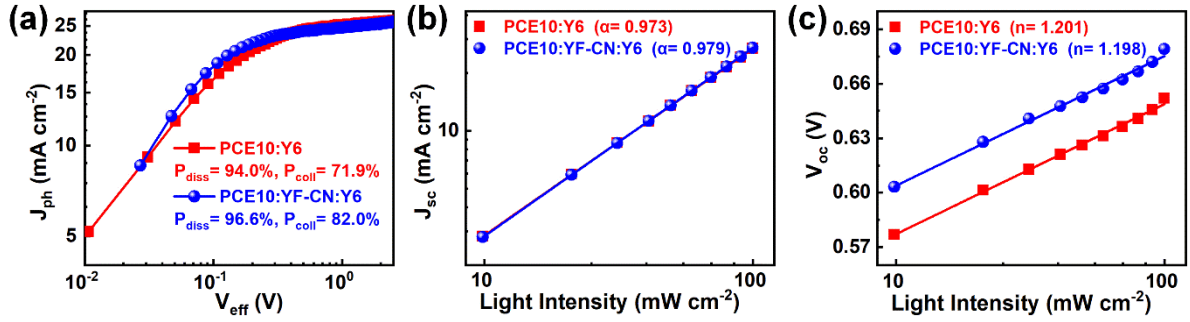


Figure 3 (a) Photocurrent density (J_{ph}) versus effective voltage (V_{eff}) curves. Dependence of (b) J_{sc} and (c) V_{oc} on the light intensity for the binary and ternary OSCs.

PCE10:YF-CN:Y6 based devices, the value of J_{sc} calculated from the integration of EQE spectra was 5.11, 5.75, 25.31 and 27.99 mA cm^{-2} , respectively, showing good consistency well with the experimental values from the J-V curves within a 5% mismatch.

The space charge limited current (SCLC) test was conducted to investigate the effect of adding YF-CN on the charge transport properties of ternary blend film. The measurement results of the electron mobilities (μ_e) and hole mobilities (μ_h) of the binary and ternary blend films are shown in **Figure S11** and summarized in **Table S2**. The μ_e and μ_h values of the PCE10:Y6 blend were calculated to be $3.22 \times 10^{-4} \text{ cm}^2\text{V}^{-1}\text{s}^{-1}$ and $2.92 \times 10^{-4} \text{ cm}^2\text{V}^{-1}\text{s}^{-1}$, respectively. With 20 wt% YF-CN in donors, the μ_e and μ_h values of the PCE10:YF-CN:Y6 (0.8:0.2:1.5) blend were increased to be $3.55 \times 10^{-4} \text{ cm}^2\text{V}^{-1}\text{s}^{-1}$ and $5.71 \times 10^{-4} \text{ cm}^2\text{V}^{-1}\text{s}^{-1}$, respectively. It is worth noting that the μ_e value of ternary active layer is almost twice as much as that of binary active layer. The improvement of charge mobility should be accountable for the higher J_{sc} values of the ternary OSCs [63].

To further investigate exciton dissociation and charge collection behavior of the devices, the relationship between photocurrent density (J_{ph}) and effective voltage (V_{eff}) of the binary and ternary OSCs were also measured and shown in **Figure 3a**. The J_{ph} is defined as $J_{ph} = J_L - J_D$, where J_L and J_D are the current density under a standard simulated light source and in dark, respectively. The V_{eff} is defined as $V_{eff} = V_0 - V_{app}$, where V_0 is the voltage at $J_{ph} = 0$ and V_{app} is the applied voltage. The larger ratios of J_{ph}/J_{sat} and $J_{max\ power}/J_{sat}$ represent more efficient exciton dissociation and charge collection efficiency respectively, in which J_{sat} is the saturated photocurrent density and $J_{max\ power}$ is the maximum power output current density [64]. The exciton dissociation probability (P_{diss}) of the PSCs, calculated from the J_{ph}/J_{sat} ratio under short circuit conditions, was increased from 94.0% to 96.6% by incorporating 20 wt% YF-CN content in donors. The charge collection probability (P_{coll}) is estimated by the ratio of $J_{max\ power}/J_{sat}$ under maximum power output conditions, which was improved from 72.0% for PCE10:Y6 device to 82.0% for PCE10:YF-CN:Y6 devices. These results

demonstrate the introduction of YF-CN helps enhance exciton dissociation and charge collection efficiency, contributing to high J_{sc} in the ternary OSCs.

To elucidate the charge recombination mechanism, light intensity (P_{light}) dependence of J_{sc} and V_{oc} for binary and ternary OSCs were measured and the results were shown in **Figure 3b** and **Figure 3c**, respectively. The dependence of J_{sc} on P_{light} can be described by the power law $J_{sc} \propto P_{light}^\alpha$, where the exponential factor α close to 1 reflects weak bimolecular recombination in the devices [65-66]. The fitting α value for the binary PCE10:Y6 and ternary devices were calculated to be 0.973 and 0.979, respectively. The larger α value indicate that the bimolecular recombination can be effectively decreased in the ternary OSCs. The correlation between V_{oc} and P_{light} can be expressed as $V_{oc} \propto (nkT/q) \ln(P_{light})$, where k is the Boltzmann constant, T is the temperature, and q is the elemental charge. In general, as the slope approaches $2kT/q$, the trap-assisted recombination is dominant in the devices [67]. The value of n was 1.201 for PCE10:Y6 device, while smaller n value of 1.198 was achieved for the ternary device, suggesting the addition of YF-CN as the third component could also suppress the trap-assisted recombination, which is consistent with the higher J_{sc} of the PCE10:YF-CN:Y6 devices.

Atomic force microscopy (AFM) was conducted to probe the surface morphology of the above active layers. The AFM height images and phase images of blend films are displayed in **Figure 4**. The root-mean-square (RMS) roughness values of PCE10:Y6 and PCE10:YF-CN film was 1.25 nm and 1.43 nm, respectively, which indicate a homogeneous surface in these blend films. The rougher morphology of YF-CN:Y6 film with 16.9 nm may be due to the crystallinity of small molecules YF-CN and Y6. More importantly, the ternary blend film of PCE10:YF-CN:Y6 displayed smaller RMS roughness value of 1.18 nm (**Figure 4d**) when introducing YF-CN into PCE10:Y6 blend. The slight decrease of roughness suggests the good compatibility among three materials, and the smooth morphology is conducive to the improvement of performances of ternary OSCs [60].

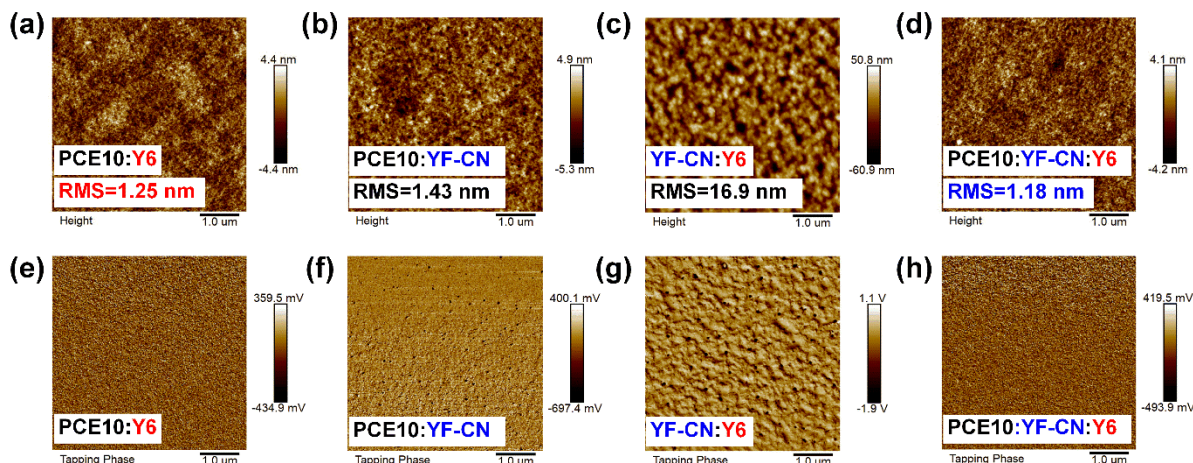


Figure 4 The AFM height images (a, b, c and d) and phase images (e, f, g and h) of as binary and ternary blend films.

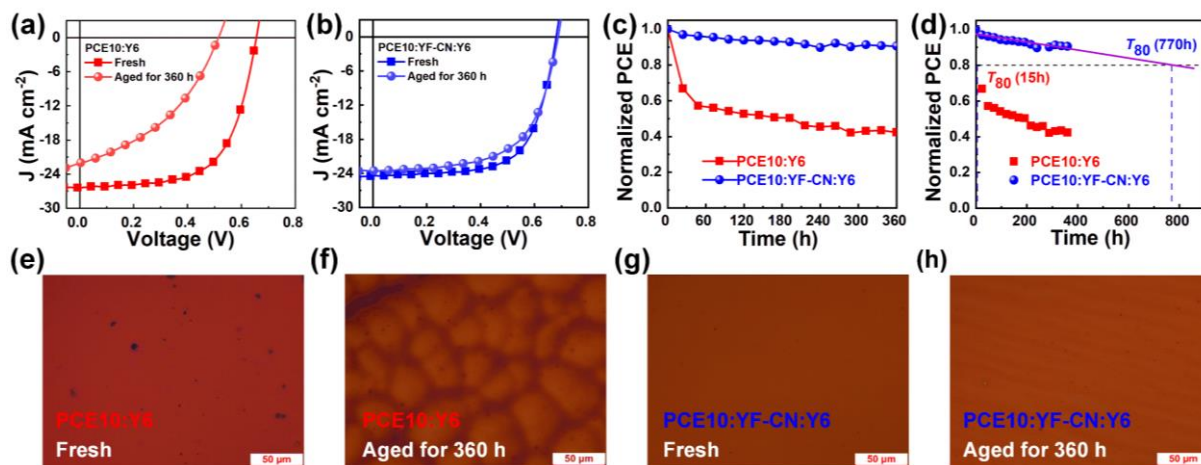


Figure 5 The J–V curves of (a) the binary and (b) ternary OSCs for fresh and aged for 360 h. (c) The storage stability of the devices at room temperature and (d) the dash line represents the T_{80} lifetime analysis of the binary and ternary devices. Fluorescence microscopy images of (e and f) the binary and (g and h) ternary OSCs for fresh and aged for 360 h.

Aside from pursuing high efficiency, the stability of devices is another important consideration for the commercialization of organic solar cells. Thus, we studied the storage stability of the binary and ternary encapsulated devices by storing in the dark in an N_2 -filled glovebox at room temperature. The devices were only exposed to light irradiation during the temporary measurements. The J–V curves of some devices are shown in **Figure 5** and the performance parameters are summarized in Table S3. As shown in **Figure 5b**, the ternary devices based on PCE10:YF-CN:Y6 system encouragingly maintained 91% of initial PCE after the 360 hours storage. In contrast, only 42% of the initial value was retained for PCE10:Y6-based binary devices under the same conditions. Furthermore, the extrapolated T_{80} (80% of the initial PCE) lifetime analysis was shown in **Figure 5c** and **Figure 5d**. The extrapolated T_{80} lifetime for the PCE10:YF-CN:Y6-based device is determined to be 770 hours, compared with the merely poor

T_{80} lifetime of 15 hours for the PCE10:Y6-based devices. These results indicate that the addition of YF-CN could significantly improve the storage stability of ternary devices. We compare the morphology of fresh and aged films of the binary and ternary, as shown in **Figure 5** and **Figure S12**. It is interesting to note that the morphology of the binary film has changed a lot but the ternary system maintains a smooth surface, which indicated that the YF-CN may work as a stabilizer by suppressing aggregation and crystallization in the ternary blend [68].

3 Conclusions

In conclusion, an IC-free small molecule YF-CN was rationally designed and readily synthesized by stille coupling. The robust carbon-carbon bonds of YF-CN enables it higher intrinsically photostability than Y6. When blending with

PCE10 or Y6, although the YF-CN based binary devices exhibited PCE about 1.4%, it exhibits an unexpected bipolar charge acceptance performance, that is, it can be either used as an electron acceptor with PCE10, or as an electron acceptor with Y6, benefiting from a more suitable energy level. Moreover, when incorporating YF-CN donor as third component into PCE10:Y6 system, the ternary as-cast device yielded a high PCE of 12.03%, which is about 20% higher than that of the binary system. The introduction of YF-CN could form a cascaded energy level alignment and improve the compatibility as well as miscibility of the ternary blend film. The ternary device showed improved storage stability due to the stable microstructure of active layer. In the future, we expect to achieve high efficiency acceptors by further molecule design to properly decrease the HOMO and LUMO level, improve the planarity of between end groups and conjugated cores and increase the absorption range covering more sunshine radiation spectra and coefficient. More experiments on both small molecules and polymers are in urgent progress in our lab on these points above. Different from the donors with open-shell structure, the highly efficient acceptors are closed-shell. Overall, this work demonstrates a promising design concept based on dinitrile end-capped closed-shell non-quinodimethane as stable active layer materials for organic solar cells.

Acknowledgments

The work was financially supported by the Natural Science Foundation of China (51973063, 21733005), the Tip-top Scientific and Technical Innovative Youth Talents of Guangdong Special Support Program (2019TQ05C890), the Ministry of Science and Technology of the People's Republic of China (2017YFA0206600), the Pearl River S&T Nova Program of Guangzhou (201710010194) and the Fund of Guangdong Provincial Key Laboratory of Luminescence from Molecular Aggregates (2019B030301003).

Conflict of interest

The authors declare that they have no conflict of interest.

Supporting information

The supporting information is available online at <http://chem.scichina.com> and <http://link.springer.com/journal/11426>. The supporting materials are published as submitted, without typesetting or editing. The responsibility for scientific accuracy and content remains entirely with the authors.

- Hou J, Inganas O, Friend R H, Gao F. *Nat Mater*, 2018, 17: 119-128.
- He Z, Zhong C, Su S, Xu M, Wu H, Cao Y. *Nature Photonics*, 2012, 6: 591-595.
- Wei Q, Liu W, Leclerc M, Yuan J, Chen H, Zou Y. *Science China Chemistry*, 2020, 63: 1352-1366.
- Liu Q, Jiang Y, Jin K, Qin J, Xu J, Li W, Xiong J, Liu J, Xiao Z, Sun K, Yang S, Zhang X, Ding L. *Science Bulletin*, 2020, 65: 272-275.
- Tong Y, Xiao Z, Du X, Zuo C, Li Y, Lv M, Yuan Y, Yi C, Hao F, Hua Y, Lei T, Lin Q, Sun K, Zhao D, Duan C, Shao X, Li W, Yip H-L, Xiao Z, Zhang B, Bian Q, Cheng Y, Liu S, Cheng M, Jin Z, Yang S, Ding L. *Science China Chemistry*, 2020, 63: 758-765.
- Yan C, Barlow S, Wang Z, Yan H, Jen A K Y, Marder S R, Zhan X. *Nature Reviews Materials*, 2018, 3: 18003.
- Lee J, Lee S M, Chen S, Kumari T, Kang S H, Cho Y, Yang C. *Adv Mater*, 2019, 31: 1804762.
- Lin Y, Wang J, Zhang Z G, Bai H, Li Y, Zhu D, Zhan X. *Adv Mater*, 2015, 27: 1170-1174.
- Yuan J, Zhang Y, Zhou L, Zhang G, Yip H-L, Lau T-K, Lu X, Zhu C, Peng H, Johnson P A, Leclerc M, Cao Y, Ulanski J, Li Y, Zou Y. *Joule*, 2019, 3: 1140-1151.
- Liu S, Yuan J, Deng W, Luo M, Xie Y, Liang Q, Zou Y, He Z, Wu H, Cao Y. *Nature Photonics*, 2020, 14: 300-305.
- Cui Y, Yao H, Zhang J, Xian K, Zhang T, Hong L, Wang Y, Xu Y, Ma K, An C, He C, Wei Z, Gao F, Hou J. *Adv Mater*, 2020, 32: 1908205.
- Wan X, Li C, Zhang M, Chen Y. *Chem Soc Rev*, 2020, 49: 2828-2842.
- Luo Z, Ma R, Liu T, Yu J, Xiao Y, Sun R, Xie G, Yuan J, Chen Y, Chen K, Chai G, Sun H, Min J, Zhang J, Zou Y, Yang C, Lu X, Gao F, Yan H. *Joule*, 2020, 4: 1236-1247.
- Ma Y, Zhang M, Wan S, Yin P, Wang P, Cai D, Liu F, Zheng Q. *Joule*, 2021, 5: 197-209.
- Li C, Zhou J, Song J, Xu J, Zhang H, Zhang X, Guo J, Zhu L, Wei D, Han G, Min J, Zhang Y, Xie Z, Yi Y, Yan H, Gao F, Liu F, Sun Y. *Nature Energy*, 2021, 6: 605-613.
- Chen S, Feng L, Jia T, Jing J, Hu Z, Zhang K, Huang F. *Science China Chemistry*, 2021, 64: 1192-1199.
- Luo Z, Sun R, Zhong C, Liu T, Zhang G, Zou Y, Jiao X, Min J, Yang C. *Science China Chemistry*, 2020, 63: 361-369.
- Bi P, Hao X. *Solar RRL*, 2019, 3: 1800263.
- Zhou D, You W, Xu H, Tong Y, Hu B, Xie Y, Chen L. *Journal of Materials Chemistry A*, 2020, 8: 23096-23122.
- An Q, Wang J, Gao W, Ma X, Hu Z, Gao J, Xu C, Hao M, Zhang X, Yang C, Zhang F. *Science Bulletin*, 2020, 65: 538-545.
- Chang Y, Zhang J, Chen Y, Chai G, Xu X, Yu L, Ma R, Yu H, Liu T, Liu P, Peng Q, Yan H. *Advanced Energy Materials*, 2021, 11: 2100079.
- Jiang M, Bai H, Zhi H, Yan L, Woo H Y, Tong L, Wang J, Zhang F, An Q. *Energy & Environmental Science*, 2021, 14: 3945-3953.
- Zeng Y, Li D, Xiao Z, Wu H, Chen Z, Hao T, Xiong S, Ma Z, Zhu H, Ding L, Bao Q. *Advanced Energy Materials*, 2021, 11: 2101338.
- Zhang M, Zhu L, Hao T, Zhou G, Qiu C, Zhao Z, Hartmann N, Xiao B, Zou Y, Feng W, Zhu H, Zhang M, Zhang Y, Li Y, Russell T P, Liu F. *Adv Mater*, 2021, 33: 2007177.
- Ma R, Tao Y, Chen Y, Liu T, Luo Z, Guo Y, Xiao Y, Fang J, Zhang G, Li X, Guo X, Yi Y, Zhang M, Lu X, Li Y, Yan H. *Science China Chemistry*, 2021, 64: 581-589.
- Gao J, Wang J, An Q, Ma X, Hu Z, Xu C, Zhang X, Zhang F. *Science China Chemistry*, 2019, 63: 83-91.
- Su Z, Zhang Z, Xie G, Zhang Y, Zhang X, Zhang W, Zhang J. *Dyes and Pigments*, 2021, 192: 109434.
- Zhang M, Zhu L, Zhou G, Hao T, Qiu C, Zhao Z, Hu Q, Larson B W, Zhu H, Ma Z, Tang Z, Feng W, Zhang Y, Russell T P, Liu F. *Nat Commun*, 2021, 12: 309.
- Liu T, Yang T, Ma R, Zhan L, Luo Z, Zhang G, Li Y, Gao K, Xiao Y, Yu J, Zou X, Sun H, Zhang M, Dela Peña T A, Xing Z, Liu H, Li X, Li G, Huang J, Duan C, Wong K S, Lu X, Guo X, Gao F, Chen H, Huang F, Li Y, Li Y, Cao Y, Tang B, Yan H. *Joule*, 2021, 5: 914-930.
- Qin J, Chen Z, Bi P, Yang Y, Zhang J, Huang Z, Wei Z, An C, Yao H, Hao X, Zhang T, Cui Y, Hong L, Liu C, Zu Y, He C, Hou J. *Energy & Environmental Science*, 2021, 14: 5903-5910.
- Xu L, Tao W, Liu H, Ning J, Huang M, Zhao B, Lu X, Tan S. *Journal of Materials Chemistry A*, 2021, 9: 11734-11740.
- Zhao C, Wang J, Zhao X, Du Z, Yang R, Tang J. *Nanoscale*, 2021, 13: 2181-2208.
- Chen Z, Song W, Yu K, Ge J, Zhang J, Xie L, Peng R, Ge Z. *Joule*, 2021, 5: 2395-2407.
- Zhang T, An C, Bi P, Lv Q, Qin J, Hong L, Cui Y, Zhang S, Hou J. *Advanced Energy Materials*, 2021, 2101705.

35. Cai Y, Li Y, Wang R, Wu H, Chen Z, Zhang J, Ma Z, Hao X, Zhao Y, Zhang C, Huang F, Sun Y. *Adv Mater*, 2021, 33: 2101733.
36. Liu F, Zhou L, Liu W, Zhou Z, Yue Q, Zheng W, Sun R, Liu W, Xu S, Fan H, Feng L, Yi Y, Zhang W, Zhu X. *Adv Mater*, 2021, 33: 2100830.
37. Bi P, Zhang S, Chen Z, Xu Y, Cui Y, Zhang T, Ren J, Qin J, Hong L, Hao X, Hou J. *Joule*, 2021, 5: 2408-2419.
38. Cui Y, Xu Y, Yao H, Bi P, Hong L, Zhang J, Zu Y, Zhang T, Qin J, Ren J, Chen Z, He C, Hao X, Wei Z, Hou J. *Adv Mater*, 2021, 33: 2102420.
39. Yu K, Song W, Li Y, Chen Z, Ge J, Yang D, Zhang J, Xie L, Liu C, Ge Z. *Small Structures*, 2021, 2100099.
40. Yamilova O R, Martynov I V, Brandvold A S, Klimovich I V, Balzer A H, Akkuratov A V, Kusnetsov I E, Stingelin N, Troshin P A. *Advanced Energy Materials*, 2020, 10: 1903163.
41. Du X, Heumueller T, Gruber W, Almora O, Classen A, Qu J, He F, Unruh T, Li N, Brabec C J. *Adv Mater*, 2020, 32: 1908305.
42. Li Y, Li T, Lin Y. *Materials Chemistry Frontiers*, 2021, 5: 2907-2930.
43. Zou Y, Ye L. *Chem*, 2021, 7: 2853-2854.
44. Ciannaruchi L, Zapata-Arteaga O, Gutiérrez-Fernández E, Martín J, Campoy-Quiles M. *Materials Advances*, 2020, 1: 2846-2861.
45. Li W, Liu D, Wang T. *Advanced Functional Materials*, 2021, 31: 2104552.
46. Liu Z X, Yu Z P, Shen Z, He C, Lau T K, Chen Z, Zhu H, Lu X, Xie Z, Chen H, Li C Z. *Nat Commun*, 2021, 12: 3049.
47. Zhu X, Liu S, Yue Q, Liu W, Sun S, Xu S. *CCS Chemistry*, 2021, 3: 1070-1080.
48. Che Y, Niazi M R, Izquierdo R, Perepichka D F. *Angew Chem Int Ed*, 2021, 60: 24833-24837.
49. Zhang Q-Q, Li Y, Wang D, Chen Z, Li Y, Li S, Zhu H, Lu X, Chen H, Li C-Z. *Bulletin of the Chemical Society of Japan*, 2021, 94: 183-190.
50. Li Y, Li L, Wu Y, Li Y. *The Journal of Physical Chemistry C*, 2017, 121: 8579-8588.
51. Chen Z, Li W, Sabuj M A, Li Y, Zhu W, Zeng M, Sarap C S, Huda M M, Qiao X, Peng X, Ma D, Ma Y, Rai N, Huang F. *Nat Commun*, 2021, 12: 5889.
52. Chen Z, Li W, Zhang Y, Wang Z, Zhu W, Zeng M, Li Y. *J Phys Chem Lett*, 2021, 12: 9783-9790.
53. Chen Z X, Li Y, Huang F. *Chem*, 2021, 7: 288-332.
54. Cheng Y-J, Yang S-H, Hsu C-S. *Chem. Rev.*, 2009, 109: 5868-5923.
55. Sun C, Qin S, Wang R, Chen S, Pan F, Qiu B, Shang Z, Meng L, Zhang C, Xiao M, Yang C, Li Y. *J Am Chem Soc*, 2020, 142: 1465-1474.
56. Yao H, Cui Y, Qian D, Ponceca C S, Jr., Honarfar A, Xu Y, Xin J, Chen Z, Hong L, Gao B, Yu R, Zu Y, Ma W, Chabera P, Pullerits T, Yartsev A, Gao F, Hou J. *J Am Chem Soc*, 2019, 141: 7743-7750.
57. Yao H, Qian D, Zhang H, Qin Y, Xu B, Cui Y, Yu R, Gao F, Hou J. *Chinese Journal of Chemistry*, 2018, 36: 491-494.
58. Cai F, Peng H, Chen H, Yuan J, Hai J, Lau T-K, Wang J, Hu Y, Liu W, Lu X, Zou Y. *Journal of Materials Chemistry A*, 2020, 8: 15984-15991.
59. Cao C, Lai H, Chen H, Zhu Y, Pu M, Zheng N, He F. *Journal of Materials Chemistry A*, 2021, 9: 16418.
60. Jiang W, Yu R, Liu Z, Peng R, Mi D, Hong L, Wei Q, Hou J, Kuang Y, Ge Z. *Adv Mater*, 2018, 30: 1703005.
61. Liu Z, Wang H. *Dyes and Pigments*, 2021, 192: 109424.
62. Jiang B-H, Chen C-P, Liang H-T, Jeng R-J, Chien W-C, Yu Y-Y. *Dyes and Pigments*, 2020, 181: 108613.
63. Ma Q, Jia Z, Meng L, Zhang J, Zhang H, Huang W, Yuan J, Gao F, Wan Y, Zhang Z, Li Y. *Nano Energy*, 2020, 78: 105272.
64. Tang H, Chen H, Yan C, Huang J, Fong P W K, Lv J, Hu D, Singh R, Kumar M, Xiao Z, Kan Z, Lu S, Li G. *Advanced Energy Materials*, 2020, 10: 2001076.
65. Chen W, Huang G, Li X, Wang H, Li Y, Jiang H, Zheng N, Yang R. *ACS Appl Mater Interfaces*, 2018, 10: 42747-42755.
66. Fukuhara T, Tamai Y, Ohkita H. *Sustainable Energy & Fuels*, 2020, 4: 4321-4351.
67. Song S, Lee K T, Koh C W, Shin H, Gao M, Woo H Y, Vak D, Kim J Y. *Energy & Environmental Science*, 2018, 11: 3248-3255.
68. Qin Y, Balar N, Peng Z, Gadisa A, Angunawela I, Bagui A, Kashani S, Hou J, Ade H. *Joule*, 2021, 5: 2129-2147.

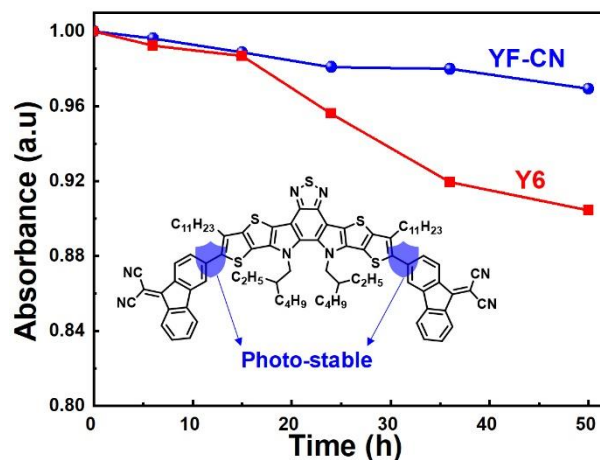


Table of Contents graphic

Supporting information

Stable dinitrile end-capped closed-shell non-quinodimethane as donor, acceptor and additive of organic solar cells

Weixuan Liang,[†] Peng Liu,[†] Yiheng Zhang, Weiya Zhu, Xinyang Tao, Zhicai He* & Yuan Li*

Institute of Polymer Optoelectronic Materials and Devices, State Key Laboratory of Luminescent Materials and Devices, South China University of Technology, Guangzhou, 510640, P.R. China,

†These authors contributed equally to this work.

E-mail: celiy@scut.edu.cn, zhicaihe@scut.edu.cn

Contents

1	Materials and instruments.....	3
2	Device fabrication and characterizations.....	3
3	Synthesis process of CN-Br and YF-CN.....	4
4	¹ H-NMR and MALDI-TOF mass spectra	6
	Figure S1. ¹ H-NMR spectrum of CN-Br in CDCl ₃	6
	Figure S2. ¹ H-NMR spectrum of CN-Br in the aromatic region in CDCl ₃	6
	Figure S3. ¹ H-NMR spectrum of YF-CN in CDCl ₃	7
	Figure S4. ¹ H-NMR spectrum of YF-CN in the aromatic region in CDCl ₃	7
	Figure S5. The high resolution MALDI-TOF mass spectrum of YF-CN.....	8
5	Additional Figures.....	8
	Figure S6. Normalized absorption spectra of YF-CN in CHCl ₃ solution and thin-film spin-coated with YF-CN in toluene solution.	8
	Figure S7. Cyclic voltammetry of (a) YF-CN and (b) Y6.	9
	Figure S8. UPS spectrum of the neat YF-CN film.	9
	Figure S9. Photoluminescence spectra of pure donor, acceptor and their blend films. (a) excited at 500 nm, (b) excited at 650 nm.....	10
	Figure S10. (a) J-V curves and (b) EQE curves of PCE10:YF-CN:Y6-based ternary devices with different blending ratios.....	11
	Figure S11. Current density-voltage curves for the (a) electron and (b) hole mobility measurements of the blend films.	12
	Figure S12. Fluorescence microscopy images in different sizes for (a, b) fresh PCE10:Y6, (e, f) aged PCE10:Y6, (c, d) fresh PCE10:YF-CN:Y6 and (g, h) aged PCE10:YF-CN:Y6.....	13
6	Additional Tables	14
	Table S1. The photovoltaic parameters of the binary and ternary OSCs with different YF-CN ratio.....	14
	Table S2. The electron mobilities (μ_e) and hole mobilities (μ_h) of the binary and ternary devices.	14
	Table S3. The photovoltaic parameters of the binary and ternary OSCs with the fresh and aged for 360 hours at room temperature.	14

1 Materials and instruments

All the chemicals and solvents were commercially available and used without further purification. PCE10 was purchased from Sigma-Aldrich and Y6 was purchased from Organtec Ltd. The nuclear magnetic resonance (NMR) spectra of the materials were measured on a Bruker AV 400 MHz spectrometer in CDCl₃ at room temperature. UV-vis absorption spectra were conducted on a UV-3600 spectrophotometer. Cyclic voltammetry of targeted films were carried out on CHI660e electrochemical workstation in electrolyte solution of 0.1 M tetrabutylammonium hexafluorophosphate (Bu₄NPF₆) by using Hg/Hg₂Cl₂ reference electrode and a platinum counter electrode, respectively.

AFM measurement: The AFM height and phase images were recorded on a Nanoscope AFM microscope (Bruker), where the tapping mode was used. The samples were fabricated in accordance with the conditions of the best devices.

SCLC measurements: Single carrier devices were fabricated, and the mobility of holes and electrons were measured by using the space charge limited current measurements. The structure of hole-only device was ITO/PEDOT:PSS/active layer/MoO₃/Ag and ITO/ZnO/active layer/PDINO/Ag for electron-only device. Analyzing in the space charge limited regime, the charge mobility is fitting by Mott-Gurney equation:

$$J = 9\varepsilon_r\varepsilon_0\mu V^2/8d^3$$

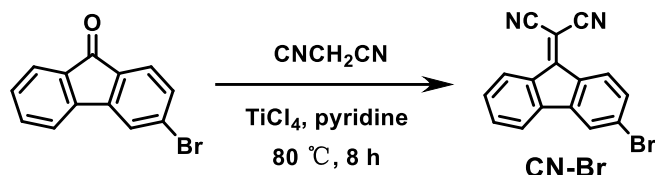
where ε_0 is the permittivity of vacuum, ε_r is the relative dielectric constant, d is the thickness of the active layer, V is the effective voltage, and μ is the mobility.

2 Device fabrication and characterizations

The organic solar cells were fabricated with a structure of ITO/PEDOT:PSS/active layer/PDINO/Ag. After 3 minutes of plasma treatment, the pre-cleaned ITO substrates were coated with 40 nm PEDOT:PSS, followed by 15 minutes annealing at 150°C. PCE10:YF-CN (1:1.5, w/w) and YF-CN:Y6 (1:1, w/w) were all dissolved in chlorobenzene at the concentration of 20 mg/mL overnight at 60 °C. PCE10:Y6 (1:1.5, w/w) and PCE10:YF-CN:Y6 (0.8:0.2:1.5, w/w) were prepared in chloroform at the concentration of 16 mg/mL and then stirred at 50°C overnight. All the solutions of active layer were spin-coated onto PEDOT:PSS layer to obtain films with a thickness of about 120 nm. The methanol solution PDINO at a concentration of 1 mg/mL was spun on top of the active layer at 3000 rpm for 40s. Finally, 100 nm Ag was deposited in

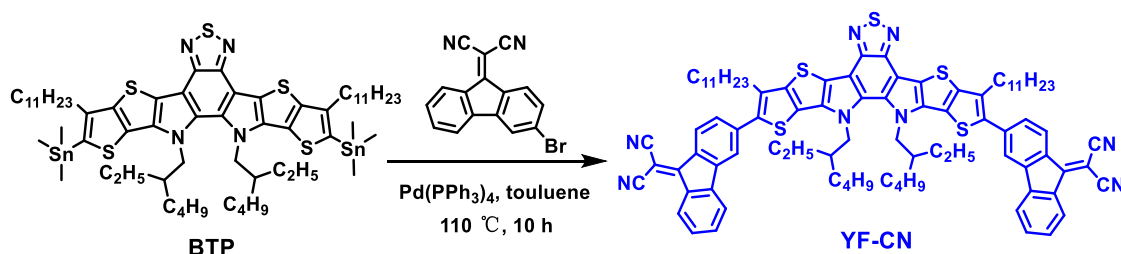
vacuum with a shadow mask at a pressure of about 3.0×10^{-4} Pa. The area of the devices was 0.057 cm^2 .

3 Synthesis process of CN-Br and YF-CN



Synthesis of 2-(3-bromo-9H-fluoren-9-ylidene)malononitrile (CN-Br)

3-Bromo-9H-fluoren-9-one (3.00 g, 0.012 mmol) and malononitrile (4.58 g, 0.07 mmol) in 30 mL of chloroform and 5 mL anhydrous pyridine under argon atmosphere, and then heated to 80°C and soaked for 0.5 h. 14 mL of chloroform solution of titanium tetrachloride (1 mol/L) was added to the reaction solution and the mixture was stirred at 80°C for 8 h. After the reaction was completed, the mixture was cooled to room temperature and extracted three times with dichloromethane. The crude product was purified by column chromatography (silica gel, petroleum ether/dichloromethane, v/v, 3:1) to afford CN-Br as a yellow-brown solid compound (3.28 g, 92.4 %). $^1\text{H-NMR}$ (CDCl_3 , 400 MHz) δ 8.40 (d, $J = 7.9$ Hz, 1H), 8.23 (d, $J = 8.4$ Hz, 1H), 7.71 (d, $J = 1.8$ Hz, 1H), 7.57-7.50 (m, 2H), 7.47 (d, $J = 8.4$, 1H), 7.40-7.35 (m, 1H).



Synthesis of YF-CN

Compound CN-Br synthesized in the previous step (45 mg, 0.148 mmol), the tin reagent BTP (80 mg, 0.062 mmol), $\text{Pd}(\text{PPh}_3)_4$ (16 mg, 0.014 mmol) and toluene (15 mL) were mixed and stirred under nitrogen atmosphere, and then heated to 110°C and soaked for 10 h. After the reaction was completed, the mixture was cooled to room temperature and extracted three times with dichloromethane. The crude product was purified by column chromatography (silica gel, petroleum ether/dichloromethane, v/v, 2:1) to afford YF-CN as a navy blue solid compound (75 mg, 85.8%). $^1\text{H-NMR}$ (CDCl_3 , 400 MHz) 8.50 (d, $J = 8.2$ Hz, 2H), 8.44 (d, $J = 7.8$ Hz, 2H), 7.75 (s, $J = 1.7$ Hz, 2H), 7.70-7.45 (m, 6H), 7.43-7.37 (m, 2H), 4.65 (m, 4H), 3.01 (m, 4H),

2.12-2.05 (m, 2H), 1.99-1.90 (m, 4H), 1.49 (m, 8H), 1.42-1.16 (m, 30H), 1.10 (m, 4H), 0.96 (m, 10H), 0.87 (m, 6H), 0.66 (m, 12H). HR-MS (MALDI-TOF) m/z calcd. for (C₈₈H₉₄N₈S₅): 1422.62. Found: 1422.76.

4 $^1\text{H-NMR}$ and MALDI-TOF mass spectra

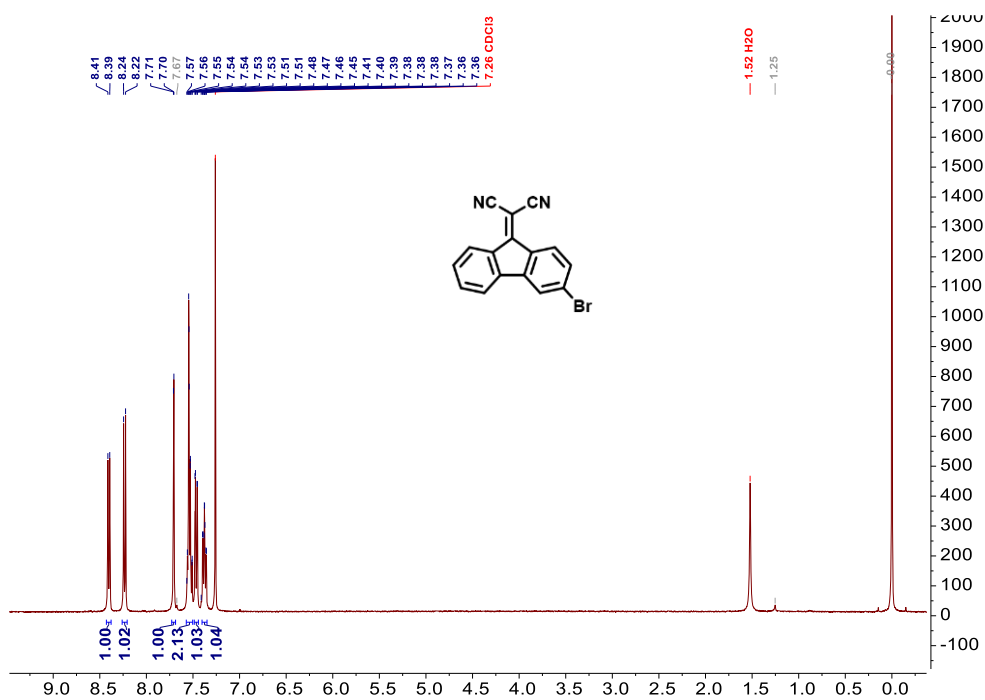


Figure S1. $^1\text{H-NMR}$ spectrum of CN-Br in CDCl_3 .

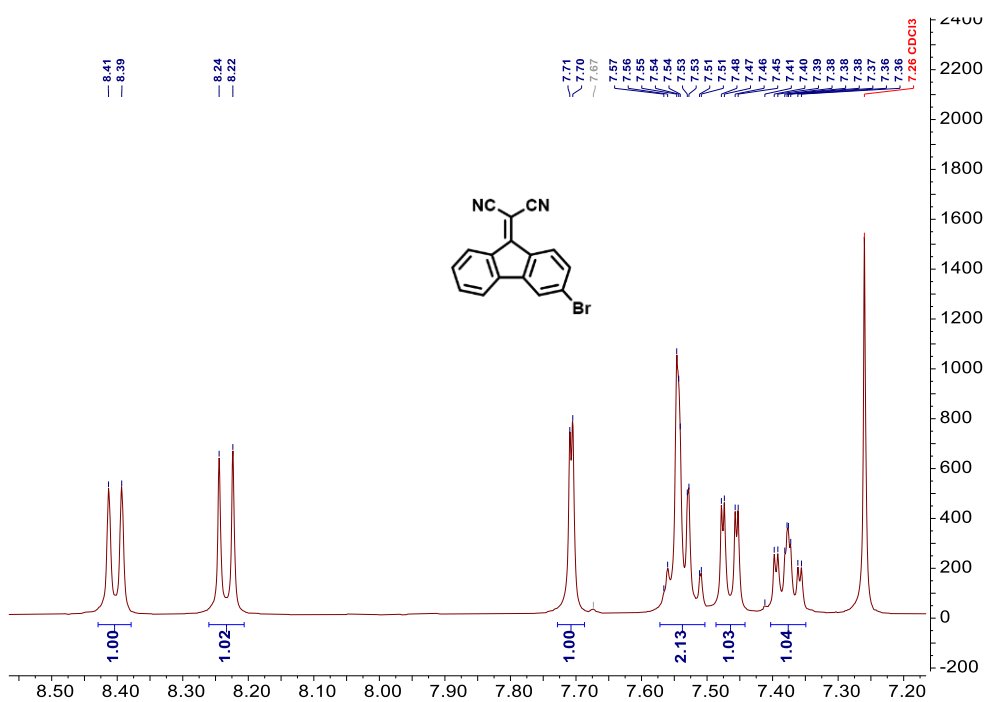


Figure S2. $^1\text{H-NMR}$ spectrum of CN-Br in the aromatic region in CDCl_3 .

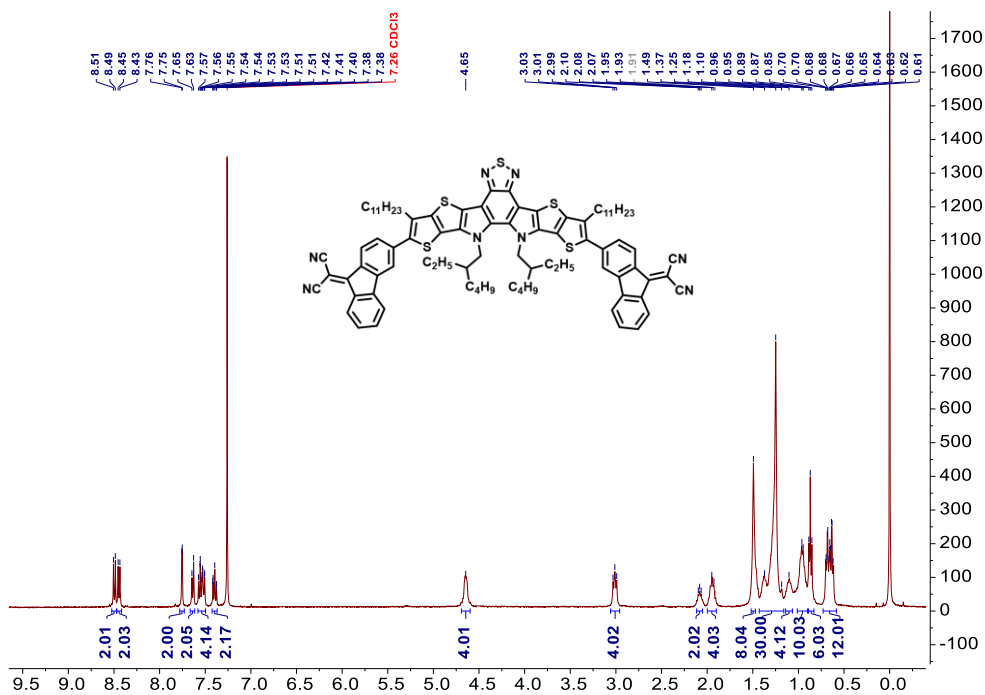


Figure S3. ¹H-NMR spectrum of YF-CN in CDCl₃.

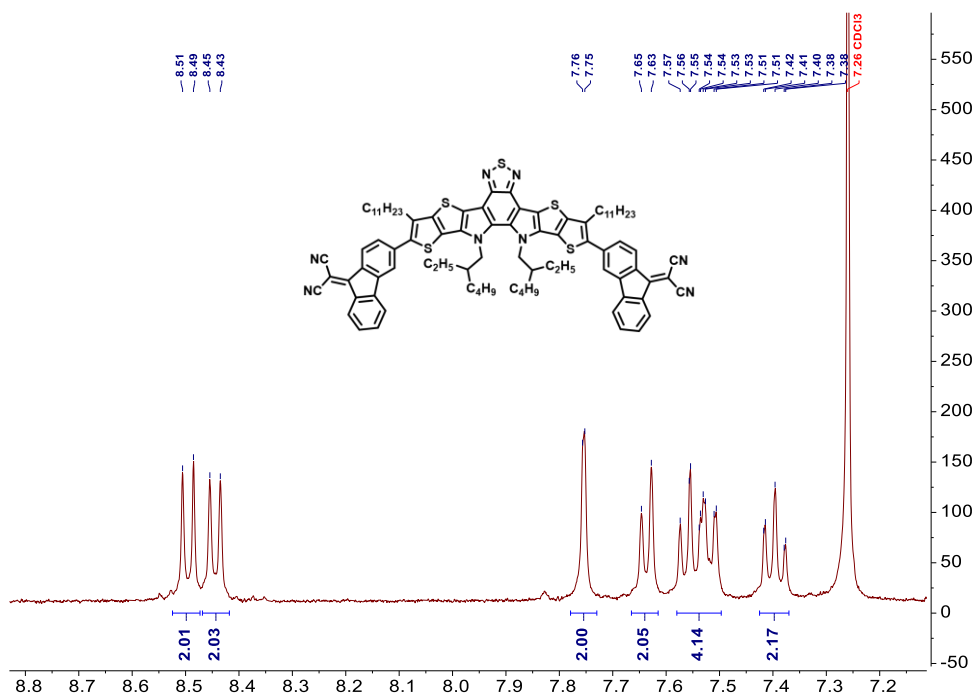


Figure S4. ¹H-NMR spectrum of YF-CN in the aromatic region in CDCl₃.

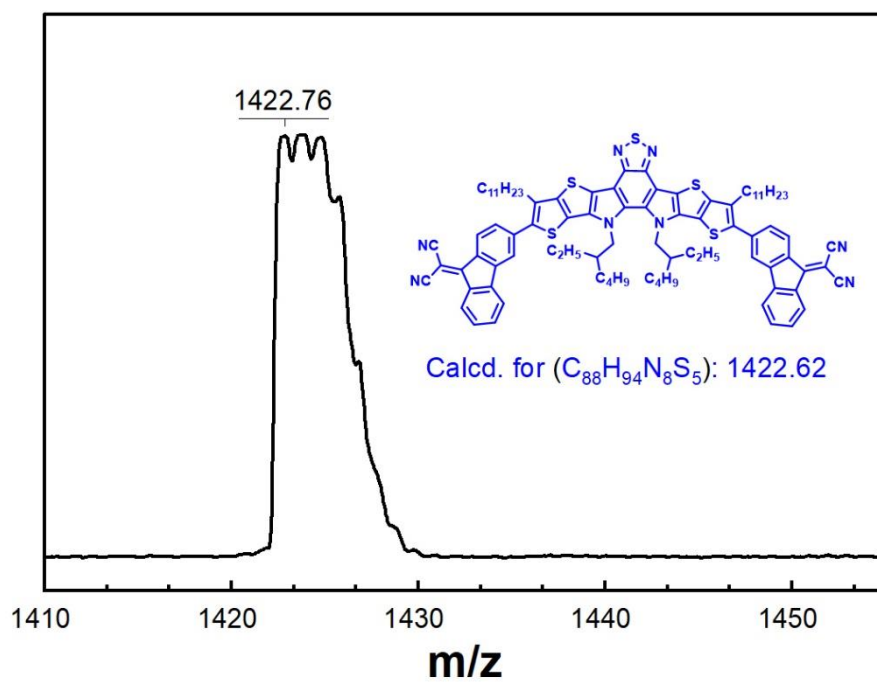


Figure S5. The high resolution MALDI-TOF mass spectrum of YF-CN.

5 Additional Figures

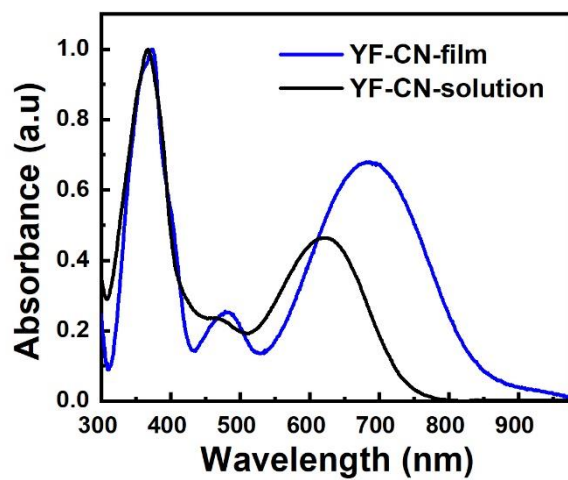


Figure S6. Normalized absorption spectra of YF-CN in CHCl₃ solution and thin-film spin-coated with YF-CN in toluene solution.

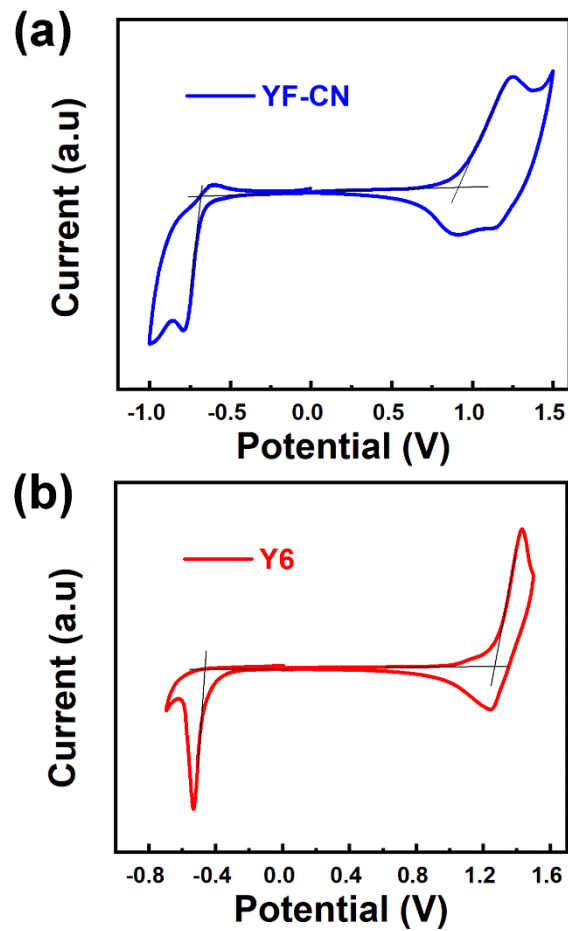


Figure S7. Cyclic voltammetry of (a) YF-CN and (b) Y6.

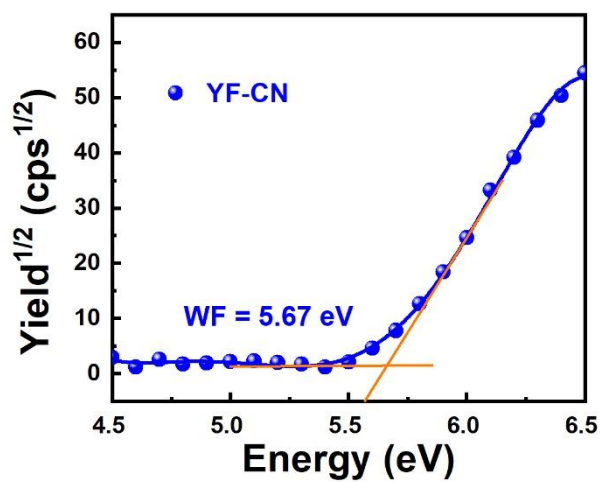


Figure S8. UPS spectrum of the neat YF-CN film.

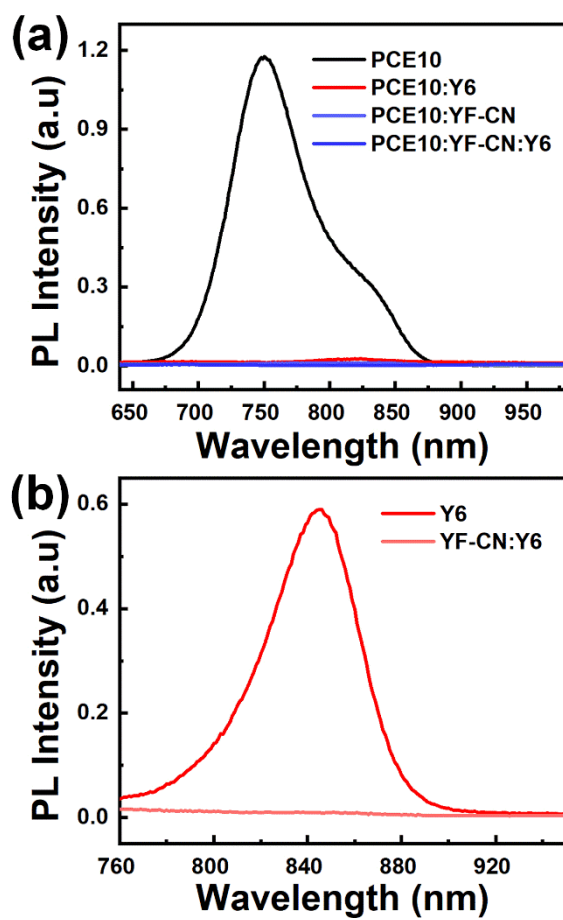


Figure S9. Photoluminescence spectra of pure donor, acceptor and their blend films. (a) excited at 500 nm, (b) excited at 650 nm.

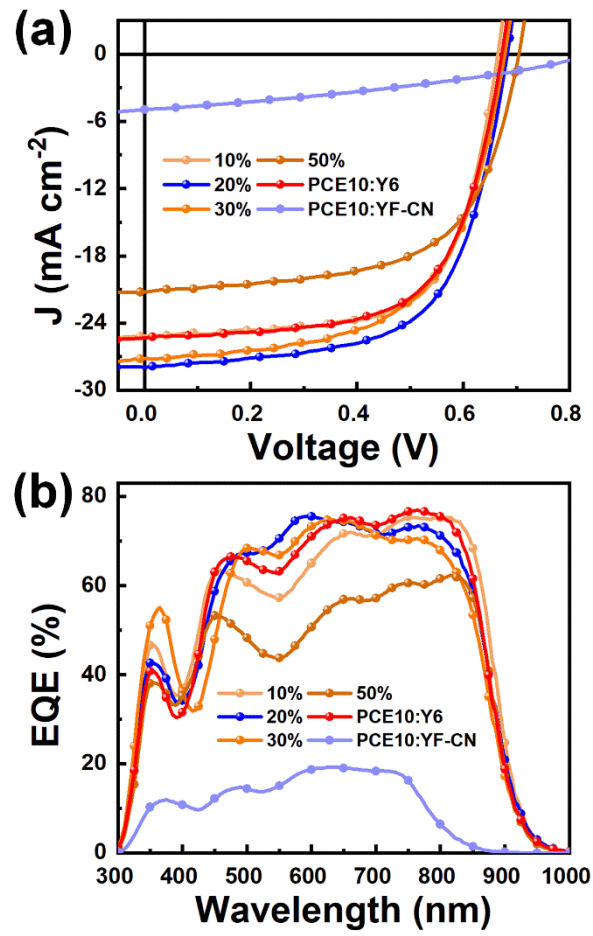


Figure S10. (a) J-V curves and (b) EQE curves of PCE10:YF-CN:Y6-based ternary devices with different blending ratios.

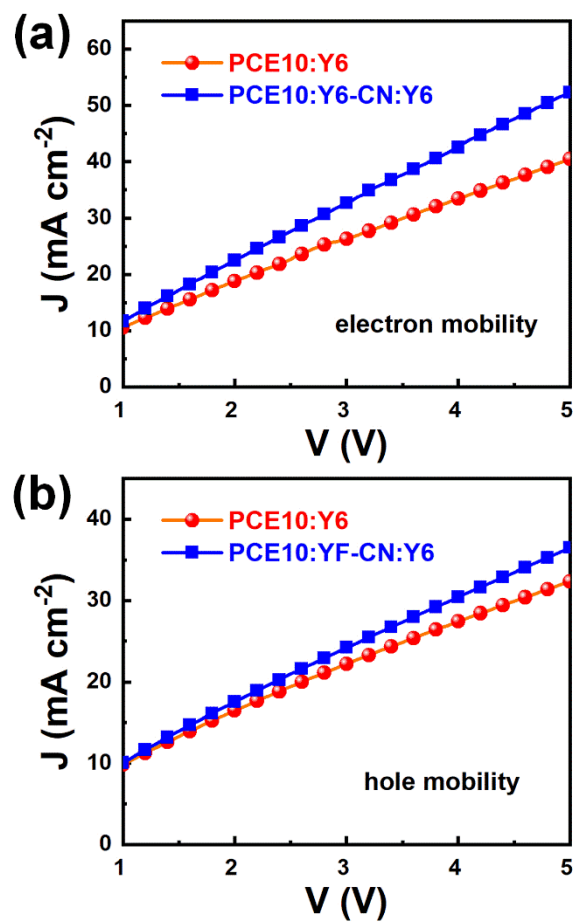


Figure S11. Current density-voltage curves for the (a) electron and (b) hole mobility measurements of the blend films.

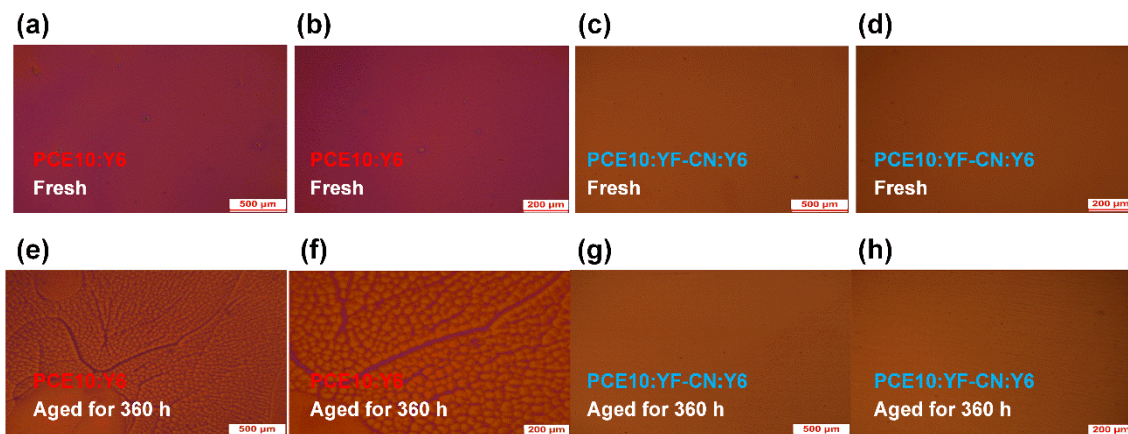


Figure S12. Fluorescence microscopy images in different sizes for (a, b) fresh PCE10:Y6, (e, f) aged PCE10:Y6, (c, d) fresh PCE10:YF-CN:Y6 and (g, h) aged PCE10:YF-CN:Y6.

6 Additional Tables

Table S1. The photovoltaic parameters of the binary and ternary OSCs with different YF-CN ratio.

Active layer	Ratio	V _{oc} (V)	J _{sc} (mA cm ⁻²)	FF (%)	PCE (%)
PCE10:Y6	1:1.5	0.673	25.32	64.19	10.93
	0.9:0.1:1.5	0.664	25.14	66.78	11.16
PCE10:YF-CN:Y6	0.8:0.2:1.5	0.683	27.92	63.11	12.03
	0.7:0.3:1.5	0.678	27.15	60.21	11.08
	0.5:0.5:1.5	0.705	21.22	61.36	9.18
PCE10:YF-CN	1:1.5	0.839	4.97	33.78	1.41

Table S2. The electron mobilities (μ_e) and hole mobilities (μ_h) of the binary and ternary devices.

	$\mu_e/10^{-4} \text{ cm}^2 \cdot \text{S}^{-1} \cdot \text{V}^{-1}$	$\mu_h/10^{-4} \text{ cm}^2 \cdot \text{S}^{-1} \cdot \text{V}^{-1}$	μ_e/μ_h
PCE10:Y6	3.22	2.92	1.10
PCE10:YF-CN:Y6	3.55	5.71	1.61

Table S3. The photovoltaic parameters of the binary and ternary OSCs with the fresh and aged for 360 hours at room temperature.

Active layer	Store Conditions	V _{oc} (V)	J _{sc} (mA cm ⁻²)	FF (%)	PCE (%)
PCE10:Y6	Fresh	0.656	26.38	62.62	10.84
	Aged for 360 h	0.515	22.07	40.28	4.58
PCE10:YF-CN:Y6	Fresh	0.681	24.40	66.26	11.01
	Aged for 360 h	0.688	23.54	61.52	9.97